

RESEARCH ARTICLE

10.1002/2015PA002834

Key Points:

- Fully coupled carbon cycle model needed when investigating carbon-calcium cycling dynamics
- Increased weathering and ocean acidification not capable of producing trends observed in Ca record
- Halt of biological export, variable Ca isotope fractionation, and input of 12,000 Pg C the most likely scenario

Supporting Information:

- Texts S1 and S2 and Figures S1–S5
- Figure S1
- Figure S2
- Figure S3
- Figure S4
- Figure S5

Correspondence to:

N. Komar,
komar@hawaii.edu

Citation:

Komar, N., and R. E. Zeebe (2016), Calcium and calcium isotope changes during carbon cycle perturbations at the end-Permian, *Paleoceanography*, 31, 115–130, doi:10.1002/2015PA002834.

Received 12 MAY 2015

Accepted 11 DEC 2015

Accepted article online 16 DEC 2015

Published online 21 JAN 2016

Calcium and calcium isotope changes during carbon cycle perturbations at the end-Permian

N. Komar¹ and R. E. Zeebe¹

¹Department of Oceanography, University of Hawaii, Honolulu, Hawaii, USA

Abstract Negative carbon and calcium isotope excursions, as well as climate shifts, took place during the most severe mass extinction event in Earth's history, the end-Permian (~252 Ma). Investigating the connection between carbon and calcium cycles during transient carbon cycle perturbation events, such as the end-Permian, may help resolve the intricacies between the coupled calcium-carbon cycles, as well as provide a tool for constraining the causes of mass extinction. Here we identify the deficiencies of a simplified calcium model employed in several previous studies, and we demonstrate the importance of a fully coupled carbon cycle model when investigating the dynamics of carbon and calcium cycling. Simulations with a modified version of the Long-term Ocean-atmosphere-Sediment CARbon cycle Reservoir model, which includes a fully coupled carbon-calcium cycle, indicate that increased weathering rates and ocean acidification (potentially caused by Siberian Trap volcanism) are not capable of producing trends observed in the record, as previously claimed. Our model results suggest that combined effects of carbon input via Siberian Trap volcanism (12,000 Pg C), the cessation of biological carbon export, and variable calcium isotope fractionation (due to a change in the seawater carbonate ion concentration) represents a more plausible scenario. This scenario successfully reconciles $\delta^{13}\text{C}$ and $\delta^{44}\text{Ca}$ trends observed in the sediment record, as well as the proposed warming of $>6^\circ\text{C}$.

1. Introduction

The calcium and carbon cycles in the ocean-atmosphere system are closely linked via weathering of carbonate and silicate rocks (sources of carbon and calcium) and calcium carbonate (CaCO_3) deposition, which is the major sink of both calcium and carbon [Ridgwell and Zeebe, 2005]. Both cycles affect oceanic alkalinity, dissolved inorganic carbon, and atmospheric CO_2 , therefore playing a major role in controlling Earth's climate [Urey, 1952; Berner, 1999]. Sharing the major sources and sinks, fluctuations in the carbon cycle (as inferred from CaCO_3 sedimentation and $\delta^{13}\text{C}$) may also be reflected in the oceanic calcium cycle and calcium isotopic composition of dissolved calcium in seawater ($\delta^{44/40}\text{Ca}_{\text{sw}} = \delta^{44}\text{Ca}_{\text{sw}}$) during major perturbations in carbon cycling [Skulan et al., 1997; Zhu and Macdougall, 1998]. Studying the connection between calcium and carbon cycling during transient carbon cycle perturbation events may help elucidate the intricacies of the coupled calcium-carbon cycles.

The largest known mass extinction of both terrestrial and marine organisms took place at the Permian-Triassic transition [Erwin, 1993], also known as the end-Permian (~252 Ma). Sedimentary records across the end-Permian show a negative excursion in the $\delta^{13}\text{C}$ of carbonate rocks [e.g., Magaritz et al., 1992; MacLeod et al., 2000; Corsetti et al., 2005], mass extinction of marine calcifiers [e.g., Knoll et al., 1996; Wignall and Newton, 2003; Knoll et al., 2007], a global temperature increase [Holser et al., 1989; Magaritz and Holser, 1991; Retallack, 1999; Sun et al., 2012], a negative excursion in calcium isotopes of marine sediments ($\delta^{44}\text{Ca}_{\text{carb}}$) [Payne et al., 2010], and a possible drop in $\delta^{44}\text{Ca}$ of seawater [Hinojosa et al., 2012] (Figure 1; $\delta^{44}\text{Ca}$ values reported are normalized to a bulk Earth standard), suggesting a carbon cycle and seawater carbonate chemistry perturbation. With the absence of pelagic calcifiers, open ocean carbonate production was essentially nonexistent during this time period [Berner, 1994; Walker et al., 2002; Erba, 2006]. Before the mass extinction event, the organisms that were capable of biogenically precipitating CaCO_3 (e.g., corals and foraminifera) were mainly confined to the shelf ocean areas, a mode of carbonate cycling also known as the "Neritan Ocean" [Zeebe and Westbroek, 2003]. These organisms suffered severe extinctions at the end-Permian, resulting in a significantly reduced biogenic carbonate production. In theory, this should create an imbalance between the input and the output of carbon and alkalinity. If imbalances persisted for a period longer than a few thousand

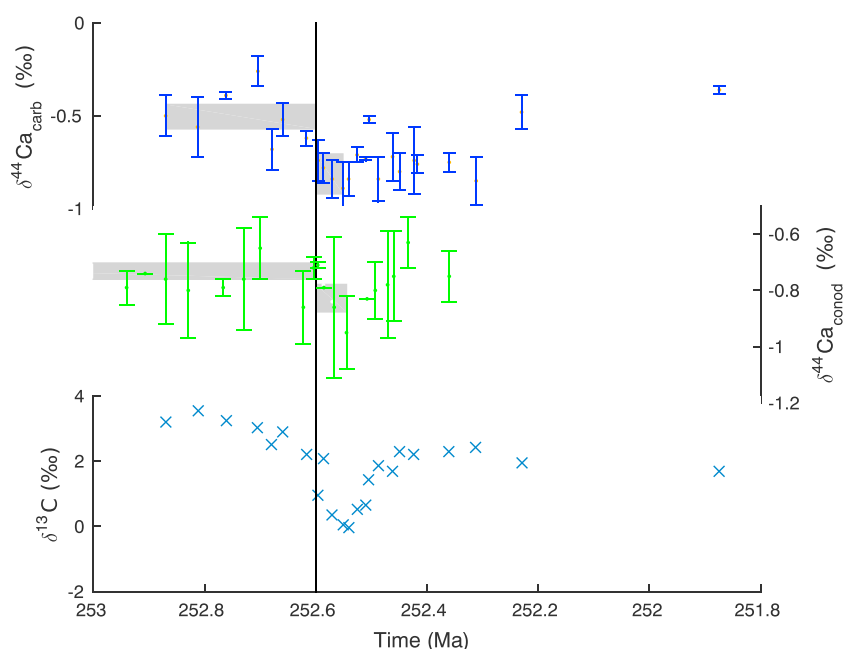


Figure 1. Calcium and carbon isotope data across the Permian-Triassic boundary. The black vertical line indicates the extinction horizon [Payne *et al.*, 2010], which corresponds to $t=0$ in LOSCAR simulations. $\delta^{44}\text{Ca}_{\text{carb}}$ and $\delta^{13}\text{C}_{\text{carb}}$ are calcium and carbon isotopic data, respectively, from marine limestone in South China reported by Payne *et al.* [2010]. $\delta^{44}\text{Ca}_{\text{conod}}$ is $\delta^{44}\text{Ca}$ of hydroxyapatite conodont microfossils measured by Hinojosa *et al.* [2012], which are indicative of seawater $\delta^{44}\text{Ca}$ (see section 6.1). $\delta^{44}\text{Ca}$ ($\delta^{44}/^{40}\text{Ca}$) values are normalized to a bulk Earth standard. The gray bands show the standard error of the mean within 95% confidence interval ($2S_e$) for the period before the extinction horizon ($\delta^{13}\text{C}_{\text{carb}}$: $-0.5 \pm 0.07\text{‰}$, $\delta^{44}\text{Ca}_{\text{conod}}$: $-0.73 \pm 0.03\text{‰}$) and during the isotope excursion ($\delta^{13}\text{C}_{\text{carb}}$: $-0.81 \pm 0.11\text{‰}$, $\delta^{44}\text{Ca}_{\text{conod}}$: $-0.83 \pm 0.05\text{‰}$).

years, the riverine input of alkalinity and carbon would exceed the output and alkalinity and carbon of the ocean would rapidly increase, leading to a decrease in atmospheric CO_2 and possibly cooling [Caldeira and Rampino, 1993]. Furthermore, depending on the duration and the magnitude of the disequilibrium, the deep ocean would eventually become supersaturated with respect to calcite. However, the evidence suggests that this was not the case during the end-Permian because temperatures rose by several degrees [Holser *et al.*, 1989; Magaritz and Holser, 1991; Retallack, 1999] while the sedimentation rates in deeper shelf sections appear to have dropped dramatically [Bowring *et al.*, 1998] indicating that there was no supersaturation with respect to calcite. Similar arguments also apply to the K/T boundary because there is no evidence for a fully saturated deep ocean or a drop in $p\text{CO}_2$ [Caldeira and Rampino, 1993] during this time period, suggesting presence of some other mechanism that keeps the ocean chemistry in balance.

The lack of evidence for large imbalances in alkalinity and carbon fluxes suggests that there has to be a mechanism that relatively quickly (on a time scale of several thousand years) compensates for the reduction in biogenically mediated carbonate precipitation, restoring the balance between inputs and outputs during the absence of biogenic carbonate production [Ridgwell *et al.*, 2003]. Caldeira and Rampino [1993] showed that during a mass extinction event (i.e., Cretaceous/Tertiary), ocean chemistry might shift so that the diminution or complete cessation in biogenic CaCO_3 production can be compensated for by a significant increase in inorganic carbonate accumulation in shallow waters, which would have important implications for the global carbon and calcium cycle and ocean carbonate chemistry. Indeed, there is a large body of evidence for Early Triassic abiotic carbonate deposition as indicated by the ubiquitous occurrence of cements, seafloor fans, stromatolites, calcified bacteria, etc. [Grotzinger and Knoll, 1995; Woods *et al.*, 1999; Ridgwell and Zeebe, 2005].

Here we employ a modified version of a one-box, calcium isotope mass-balance model constructed by Payne *et al.* [2010] to study the possible effects of a major carbon perturbation accompanied by mass extinction of biota (such as the end-Permian) on ocean carbonate chemistry and the marine calcium cycle. We also point out problems in the assumptions made in the original model by Payne *et al.* [2010] pertaining to the shallow-water carbonate compensation mechanism explained above. Next, we utilize the Long-term

Table 1. Parameter Values Used in the Model^a

Parameter	Value	Unit	References
$[Ca^{2+}]_0$	10	mmol kg ⁻¹	<i>Horita et al.</i> [2002]
F_{riv}	14	10 ¹² mol Ca yr ⁻¹	<i>Pilson</i> [2012]
F_{hyd}	4	10 ¹² mol Ca yr ⁻¹	<i>Elderfield and Schultz</i> [1996]
F_{pw}	6.3	10 ¹² mol Ca yr ⁻¹	<i>Pilson</i> [2012]
k_{carb}	24.3	10 ¹² mol Ca yr ⁻¹	calculated to balance fluxes
F_{carb}	see equation (2)	10 ¹² mol Ca yr ⁻¹	<i>Payne et al.</i> [2010]
δ_{sw}	0.9	‰	Steady-state value with $\epsilon = 1.4‰$
δ_{riv}	-0.6	‰	Assumes that carbonate weathering is predominant source of Ca [<i>Fantle and Tipper</i> , 2014]
δ_{hyd}	-0.25	‰	<i>Amini et al.</i> [2008]
δ_{pw}	-0.45	‰	<i>Payne et al.</i> [2010]
ϵ_{carb}	-1.4	‰	<i>Fantle and DePaolo</i> [2007]

^a $\delta^{44}Ca$ values are normalized to a bulk Earth standard.

Ocean-atmosphere-Sediment Carbon cycle Reservoir model (LOSCAR) [*Zeebe*, 2012] that has been expanded to trace $[Ca^{2+}]$ and $\delta^{44}Ca$ in the ocean (in both sediments and seawater), i.e., a fully coupled C-Ca model. This allows us to perform more sophisticated analyses of carbon and calcium cycle dynamics and resulting changes in seawater carbonate chemistry.

2. Calcium-Only Model

The model of *Payne et al.* [2010] consists of a single ocean box. The calcium fluxes to the ocean are river input (F_{riv}), hydrothermal alteration (F_{hyd}), and pore water flux (F_{pw}). Calcium is removed from the ocean via burial of carbonate minerals (F_{carb}). The following equation describes the change in calcium concentration (M_{Ca}) over time:

$$\frac{dM_{Ca}}{dt} = F_{riv} + F_{hyd} + F_{pw} - F_{carb}. \quad (1)$$

Values for F_{riv} , F_{hyd} , and F_{pw} are prescribed (see Table 1), while the burial of carbonate is calculated as the square of the ratio between the current ($[Ca^{2+}]_t$) and steady state calcium concentration ($[Ca^{2+}]_0$):

$$F_{carb} = k_{carb} \times \left(\frac{[Ca^{2+}]_t}{[Ca^{2+}]_0} \right)^2 \quad (2)$$

where k_{carb} is a scaling constant. It is important to note that this approach assumes a constant carbonate ion concentration. Each of the fluxes has a calcium isotope composition ($\delta^{44}Ca$) with values presented in Table 1. This allows modeling of the changes in $\delta^{44}Ca_{sw}$ using the following equation:

$$\frac{d(M_{Ca}\delta_{sw})}{dt} = F_{riv} \times (\delta_{riv} - \delta_{sw}) + F_{hyd} \times (\delta_{hyd} - \delta_{sw}) + F_{pw} \times (\delta_{pw} - \delta_{sw}) - F_{carb} \times \epsilon_{carb} \quad (3)$$

where δ_{sw} , δ_{riv} , δ_{hyd} , and δ_{pw} are the $\delta^{44}Ca$ of seawater, river, hydrothermal input, and pore water fluxes, respectively. ϵ_{carb} is the fractionation factor between seawater and buried carbonates.

Equations (1) and (3) are solved numerically by running the model forward in time over four million years. In order to replicate the end-Permian acidification scenario, which is the preferred scenario proposed by *Payne et al.* [2010] and *Hinojosa et al.* [2012], the carbonate burial flux was decreased by 17.7% while simultaneously increasing the riverine input by a factor of 3.3 over 100 kyr (Figure 2). This was justified by *Payne et al.* [2010] who argued that during ocean acidification the carbonate burial flux decreases and then subsequently increases due to weathering feedbacks. These forcing values were chosen in order to replicate the $\delta^{44}Ca$ trend and the duration observed in the sediment record ($\delta^{44}Ca_{carb}$), which suggests a negative excursion of about 0.3‰. Note that 0.3‰ is the full excursion from mean uppermost Permian values of $\sim -0.5‰$ (Figure 1) to

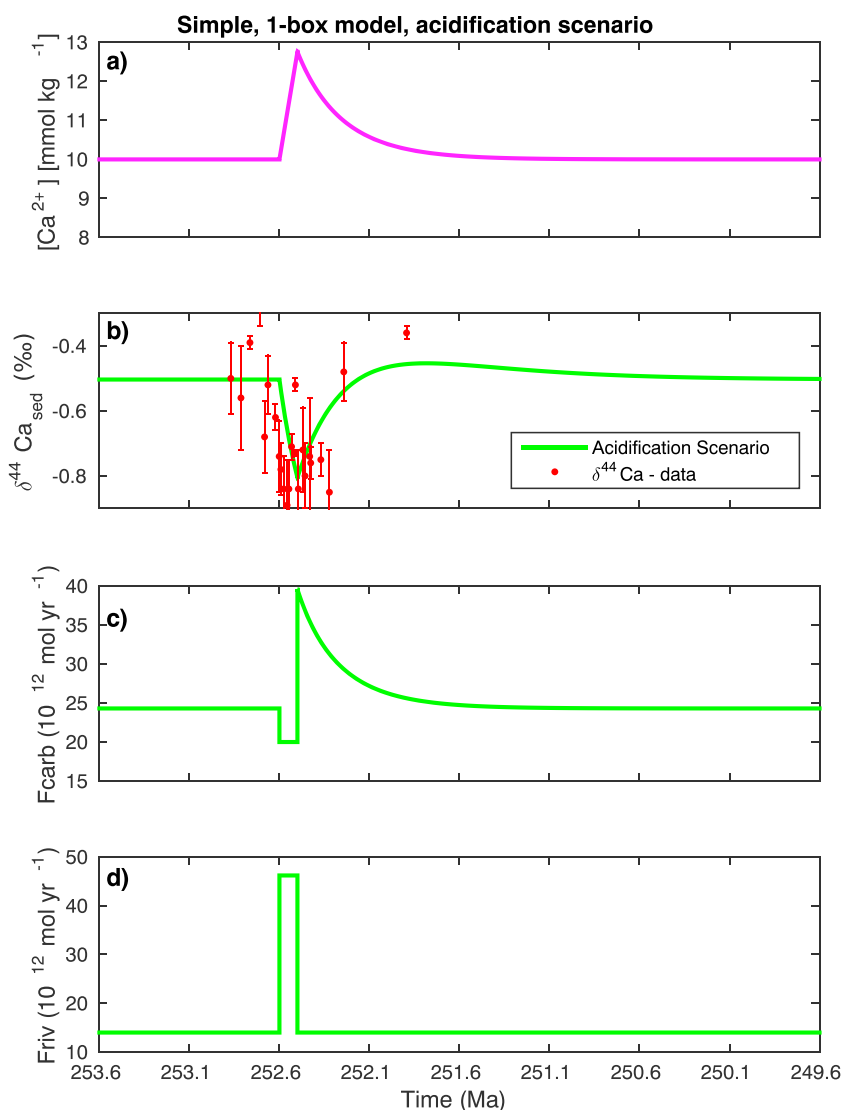


Figure 2. Accelerated weathering and reduced burial simulation. This is the preferred scenario of Payne *et al.* [2010]. The model was forced by enhancing the riverine flux by a factor of 3.3 times the initial value over 100 kyr while at the same time reducing carbonate burial by 17.7%. (a) Calcium ion concentration. (b) Calcium isotope response of buried carbonates. (c) Carbonate burial flux. (d) Riverine flux of calcium.

the minimum value of about -0.8‰ at the end of extinction horizon. The excursion from $t = 0$ (the extinction horizon) to the minimum value is about 0.2‰ , which is used as the target in our LOSCAR simulations.

However, while we recognize the desire for simplicity, there are problems with this approach. First, the shape of the riverine perturbation is not realistic. An abrupt increase in weathering rates, subsequently remaining elevated for 100 kyr, followed by an instantaneous cessation and recovery back to pre-perturbation levels is very unlikely (Figure 2d) as the change in weathering is expected to be more gradual in either direction. Second, the feedback between carbonate burial and $[\text{Ca}^{2+}]$ described in equation (2) is not used during the perturbation period. The carbonate burial is instead simply prescribed, essentially decoupling inputs and outputs of calcium. Therefore, the only sink of carbonate in this model becomes independent of both riverine fluxes and seawater $[\text{Ca}^{2+}]$.

The prescribed reduction in burial was used to simulate acidification (by reducing burial by 17.7% over 100 kyr), which also contributes to an additional negative excursion in $\delta^{44}\text{Ca}$. However, it is important to note that even without this prescribed reduction in burial, the $\delta^{44}\text{Ca}_{\text{carb}}$ drops by about 0.27‰ due to the increased riverine

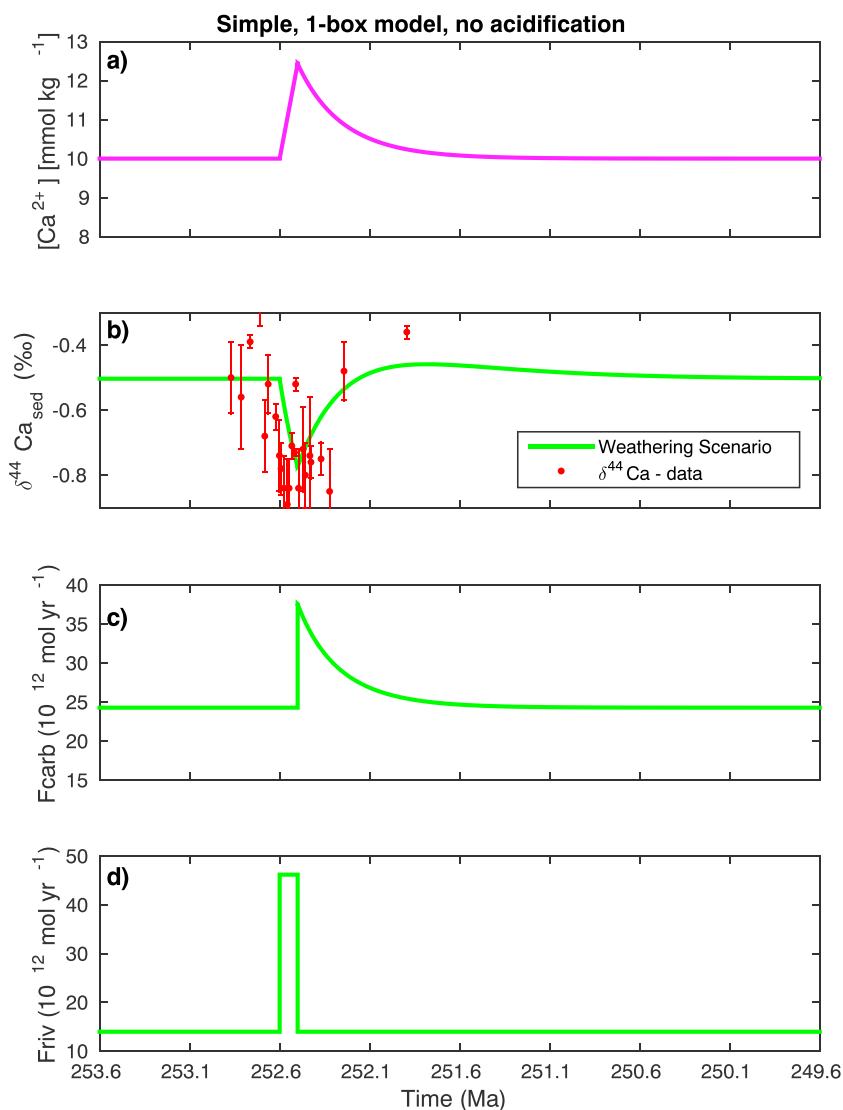


Figure 3. Accelerated weathering-only scenario (no reduced burial). The riverine forcing used is the same as in Figure 2. (a) Calcium ion concentration. (b) Calcium isotope response of buried carbonates. (c) Carbonate burial flux. (d) Riverine flux of calcium.

flux alone (Figure 3). In this simulation, the change in carbonate burial (Figure 3c) is governed by the change in $[Ca^{2+}]$ as described in equation (2).

Most importantly, the model does not account for changes in $[CO_3^{2-}]$. On the time scale of the perturbation it is essential to account for changes in $[CO_3^{2-}]$ because the compensation e -folding time of the carbonate ion concentration in seawater is about 6000 to 10,000 years. This means that the response time of carbonate ion is quick relative to a ~ 100 kyr perturbation. Therefore, on time scales of hundreds of thousands of years it appears unrealistic to decouple the weathering and carbonate burial. For this reason the model presented in Payne *et al.* [2010] has been expanded to account for changes in the carbonate ion concentration of seawater.

3. Calcium and Carbonate Ion Model

As explained above, the major shortcoming of the calcium-only model is that it neglects changes in $[CO_3^{2-}]$, which is essential, however, for calculating shallow water carbonate production/deposition. This drawback

Table 2. Additional Parameters Used in the Expanded Calcium Model, Which Accounts for the Change in $[\text{CO}_3^{2-}]$ and Calcite Saturation State

Parameter	Value and Unit	Notes
Temperature	20°C	
Salinity	35	
Pressure	15 bar	shallow ocean
K_{sp}^*	4.4×10^{-7}	based on T, S, P , and initial $[\text{Mg}^{2+}]$ and $[\text{Ca}^{2+}]$
k_{cr}	$10.8 \times 10^{12} \text{ mol yr}^{-1}$	calculated to balance fluxes
$[\text{CO}_3^{2-}]_0$	$180 \mu\text{mol kg}^{-1}$	arbitrary, see text
Ω_0	4	calculated initial calcite saturation state

can be easily rectified by introducing an additional equation to the model tracing $[\text{CO}_3^{2-}]$ in the ocean over time, as described in Zeebe and Westbroek [2003]:

$$\alpha M_{OC} \frac{d[\text{CO}_3^{2-}]}{dt} = F_{rivC} - F_{carb} \quad (4)$$

where M_{OC} is the mass of the ocean ($1.4 \times 10^{21} \text{ kg}$), α is a factor that accounts for the buffer capacity of seawater ($\alpha \approx 2$), and F_{rivC} is the total CO_3^{2-} input. The α factor takes into account that the dissolution or precipitation of one mole of CaCO_3 changes $[\text{CO}_3^{2-}]$ by roughly half a mole. The main implicit assumption in equation (4) is that any imbalance between riverine input of calcium and calcium burial also represents an imbalance of carbon fluxes. In other words, calcium and carbon are weathered/buried in a 1:1 molar ratio. Because this ratio is 1:1, the only way to balance CO_3^{2-} and calcium fluxes in this simple model is to assume that Ca^{2+} and CO_3^{2-} influx are equal ($F_{rivC} = F_{riv} + F_{hyd} + F_{pw}$).

Since now both $[\text{CO}_3^{2-}]$ and $[\text{Ca}^{2+}]$ are predicted by the model, the carbonate saturation state (Ω) of seawater can be calculated:

$$\Omega = \frac{[\text{Ca}^{2+}]_{sw} \times [\text{CO}_3^{2-}]_{sw}}{K_{sp}^*} \quad (5)$$

where $[\text{Ca}^{2+}]_{sw}$ and $[\text{CO}_3^{2-}]_{sw}$ are the in situ concentration of Ca^{2+} and CO_3^{2-} in seawater, respectively. K_{sp}^* is the solubility product of calcite at the in situ temperature, salinity, and pressure (see Table 2). Knowing Ω allows for calculation of precipitation rates of inorganic calcite in shallow water according to the following [Caldeira and Rampino, 1993; Zeebe and Westbroek, 2003; Ridgwell et al., 2003; Rampino and Caldeira, 2005]:

$$F_{carb} = k_{cr} \times (\Omega - 1)^\eta \quad (6)$$

where k_{cr} is a rate constant (for values see Table 2), set to balance fluxes at the initial steady state, and η is the order of reaction (set to $\eta = 2$) [see, e.g., Caldeira and Rampino, 1993; Opdyke and Wilkinson, 1993; Zeebe and Westbroek, 2003].

As pointed out earlier, the $\delta^{44}\text{Ca}_{carb}$ in the preferred scenario (Figure 2b) of Payne et al. [2010] is mostly controlled by the weathering flux rather than acidification. By “turning off” acidification, 90% of the $\delta^{44}\text{Ca}_{carb}$ signal is still preserved (Figure 3b). Having $[\text{CO}_3^{2-}]$ as an additional tracer and the carbonate burial feedback as described above, a new simulation was performed (Figure 4) in order to investigate how the system responds to increased weathering fluxes with a proper burial feedback. In order to demonstrate the significance of $[\text{CO}_3^{2-}]$ on $\delta^{44}\text{Ca}_{carb}$, a new simulation (Figure 4) was run with the same forcing as in Figure 3 (F_{riv} increased by 3.3 times over 100 kyr). Because carbonate burial now depends on the calcite saturation state, the burial flux (Figure 4c) responds more quickly to the perturbation and closely follows the shape of the riverine flux (Figure 4d). As a consequence, changes in $[\text{Ca}^{2+}]$ and $\delta^{44}\text{Ca}_{carb}$ are dampened by an order of magnitude when compared to the simulation shown in Figure 3. The oceanic calcium concentration changes by only $0.14 \mu\text{mol kg}^{-1}$ and the $\delta^{44}\text{Ca}_{carb}$ excursion is only about 0.03‰ (about 7 times smaller than implied by the data).

The initial $[\text{CO}_3^{2-}]$ ($180 \mu\text{mol kg}^{-1}$) was chosen arbitrarily in order to produce shallow water initially supersaturated with respect to calcite ($\Omega \approx 4$). The actual shallow water concentration of CO_3^{2-} during the end-Permian

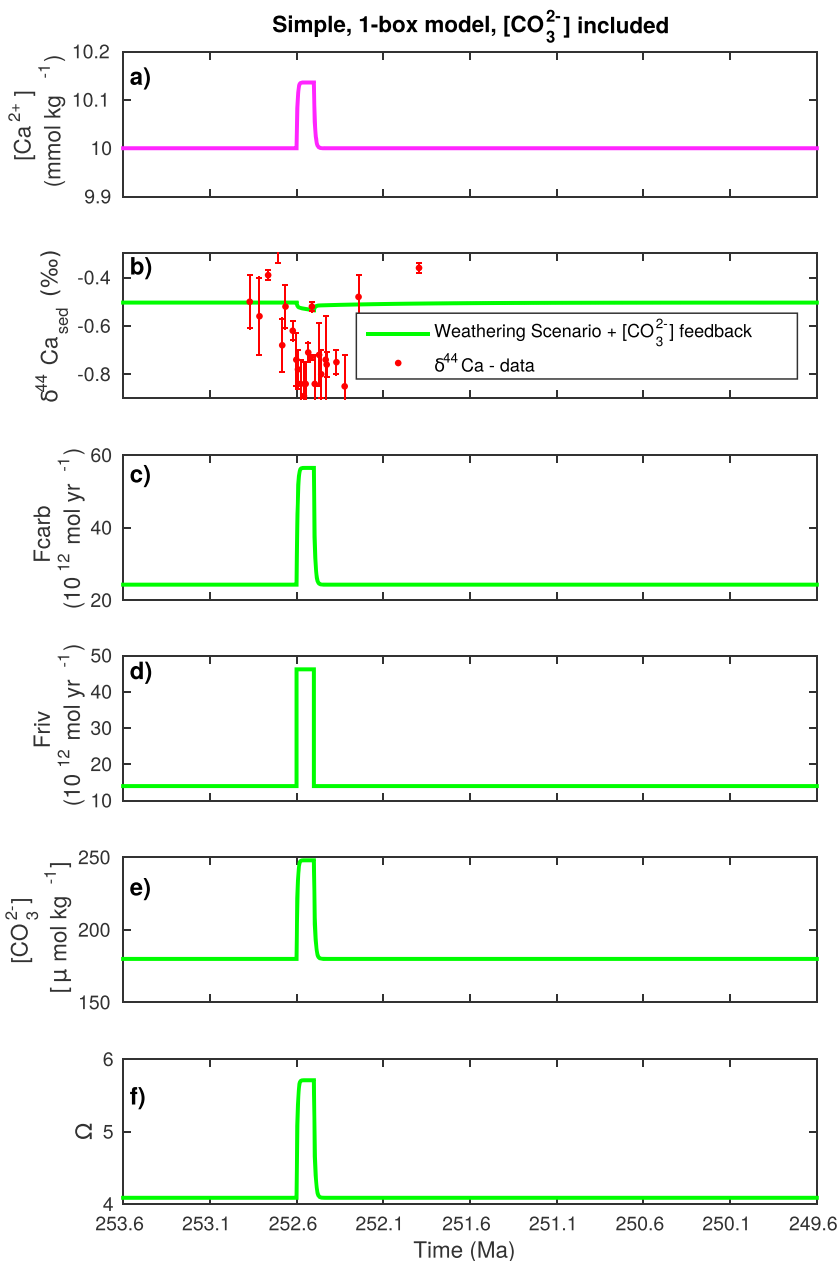


Figure 4. Model results using the calcite saturation state (Ω) in the carbonate weathering feedback. The riverine forcing used is the same as in Figures 2 and 3. (a) Calcium ion concentration. (b) Calcium isotope response of buried carbonates. (c) Carbonate burial flux. (d) Riverine flux of calcium. (e) Carbonate ion concentration. (f) Calcite saturation state.

is unknown, but assuming any two components of the ocean CO_2 system, it can be calculated [Zeebe and Wolf-Gladrow, 2001]. Because there is little or no direct way of knowing any component of the CO_2 system during the end-Permian, the dissolved inorganic carbon (DIC) and pH values estimated by the Earth system model described in Ridgwell [2005] were used. Ridgwell [2005] suggests a DIC concentration of about $4000 \mu\text{mol kg}^{-1}$ and pH of about 7.7. Note that for the same DIC and $[\text{CO}_3^{2-}]$ the Ω calculated in this study ($\Omega=4$) is lower than the one in Ridgwell [2005, $\Omega \sim 5.5$]. This is due to the fact that we use a lower $[\text{Ca}^{2+}]$ here in order to be consistent with the model results presented in Payne et al. [2010].

There is a large uncertainty associated with initial $[\text{CO}_3^{2-}]$ and therefore Ω during the studied time period. However, additional model runs (not shown) revealed that the change in $\delta^{44}\text{Ca}_{\text{carb}}$ is not very sensitive to the initial $[\text{CO}_3^{2-}]$. For example, doubling the initial $[\text{CO}_3^{2-}]$ produces a greater negative excursion ($\sim 0.05\text{‰}$) in

$\delta^{44}\text{Ca}_{\text{carb}}$ but still not nearly enough to explain the observation. According to our simulations and sensitivity studies, it appears that an accelerated weathering event on time scales of hundreds of thousands of years is not capable of producing significant changes in the calcium cycle (i.e., seawater $[\text{Ca}^{2+}]$ and Ca isotope ratio).

4. LOSCAR Simulations

In order to perform a more sophisticated analysis, we also used an expanded version of the LOSCAR model. A detailed, comprehensive description of the LOSCAR model (Figure S1 in the supporting information), its components and architecture is given in Zeebe [2012]. Here we only describe main modifications made in the model as well as updated boundary conditions, which pertain to the end-Permian. A similar LOSCAR version that includes Ca^{2+} as a tracer was used and described in Komar and Zeebe [2011] with the exception that now the model also includes the distribution of stable calcium isotopes ($\delta^{44}\text{Ca}$), thus, integrating fully coupled carbon and calcium cycles.

The model was modified in order to reflect the changes associated with a mass extinction across the end-Permian. Accordingly, the pre-steady state pelagic biological CaCO_3 rain is set to zero. CaCO_3 is precipitated exclusively over the shallow sediment boxes (driven by saturation state; equation (6)), rendering the deep sediments free of calcite, meaning that calcite is accumulated only in shallow waters. The calculated shelf area is $\sim 30 \times 10^6 \text{ km}^2$, which is approximately equal to the shelf ocean area during the Late Permian [Osen et al., 2013]. The rate of inorganic precipitation of CaCO_3 depends on the calcite saturation state, the same way it does in the simple calcium and carbonate model as described by equation (6).

Model time $t = 0$ corresponds to end-Permian extinction horizon ($\sim 252.6 \text{ Ma}$). The initial atmospheric $p\text{CO}_2$ used in all LOSCAR simulations is set to $850 \mu\text{atm}$. This CO_2 concentration is within the range of values reconstructed from proxy records and other modeling studies [Berner, 1994; Royer et al., 2004; Cui and Kump, 2015] for this time period. The low-latitude surface ocean temperature is set to 25°C [Sun et al., 2012]. Temperature sensitivity to doubling of CO_2 was set to 3°C . Silicate and carbonate weathering fluxes were set so that the initial cumulative riverine input ($14 \times 10^{12} \text{ mol yr}^{-1}$) equals that of the simple calcium model [Payne et al., 2010]. Additionally, for consistency and easier comparison with the simple model, the initial $[\text{Ca}^{2+}]$ was set to 10 mmol kg^{-1} , which is in line with the fluid inclusions data for this time period [Horita et al., 2002]. Nevertheless, we tested the model sensitivity to different Ca concentrations (see section 6.1 and supporting information). Carbonate and silicate weathering fluxes of calcium are set to the same isotopic value of -0.6‰ . The model calculates ocean carbonate chemistry parameters (e.g., $[\text{CO}_2]$, $[\text{CO}_3^{2-}]$, pH) from total carbon and total alkalinity using routines described in Zeebe and Wolf-Gladrow [2001] and Zeebe [2012]. These routines allow for variations in the Ca^{2+} concentration of seawater, which is critical for paleo-ocean carbonate chemistry reconstructions. This is important because the concentration of calcium affects the thermodynamics (e.g., equilibrium constants and solubility products), which in turn affects the predicted ocean carbonate chemistry and atmospheric $p\text{CO}_2$.

5. Comparison: Simple Model Versus LOSCAR

As noted above, both the simple calcium carbonate ion model and LOSCAR use the same feedback for calculating calcite precipitation, which is governed by equation (6). Nevertheless, the two models produce significantly different results (e.g., compare Figures 4 and 5). The core of this discrepancy is the fact that the two models utilize different forcings. The simple calcium model is simply driven by prescribing an increase in riverine flux (simulating accelerated weathering), whereas in LOSCAR the system is perturbed by adding a large amount of carbon to the ocean-atmosphere reservoir. This addition of carbon drives the atmospheric CO_2 upward. Observations indicate that the increase in $p\text{CO}_2$ (and consequently temperature and precipitation) results in enhanced weathering of carbonate and silicate rocks. In LOSCAR, this is parameterized as follows:

$$F_{\text{Si}} = F_{\text{Si}}^0 \times \left(\frac{p\text{CO}_2}{p\text{CO}_2^0} \right)^{n_{\text{Si}}} \quad (7)$$

$$F_{\text{C}} = F_{\text{C}}^0 \times \left(\frac{p\text{CO}_2}{p\text{CO}_2^0} \right)^{n_{\text{CC}}} \quad (8)$$

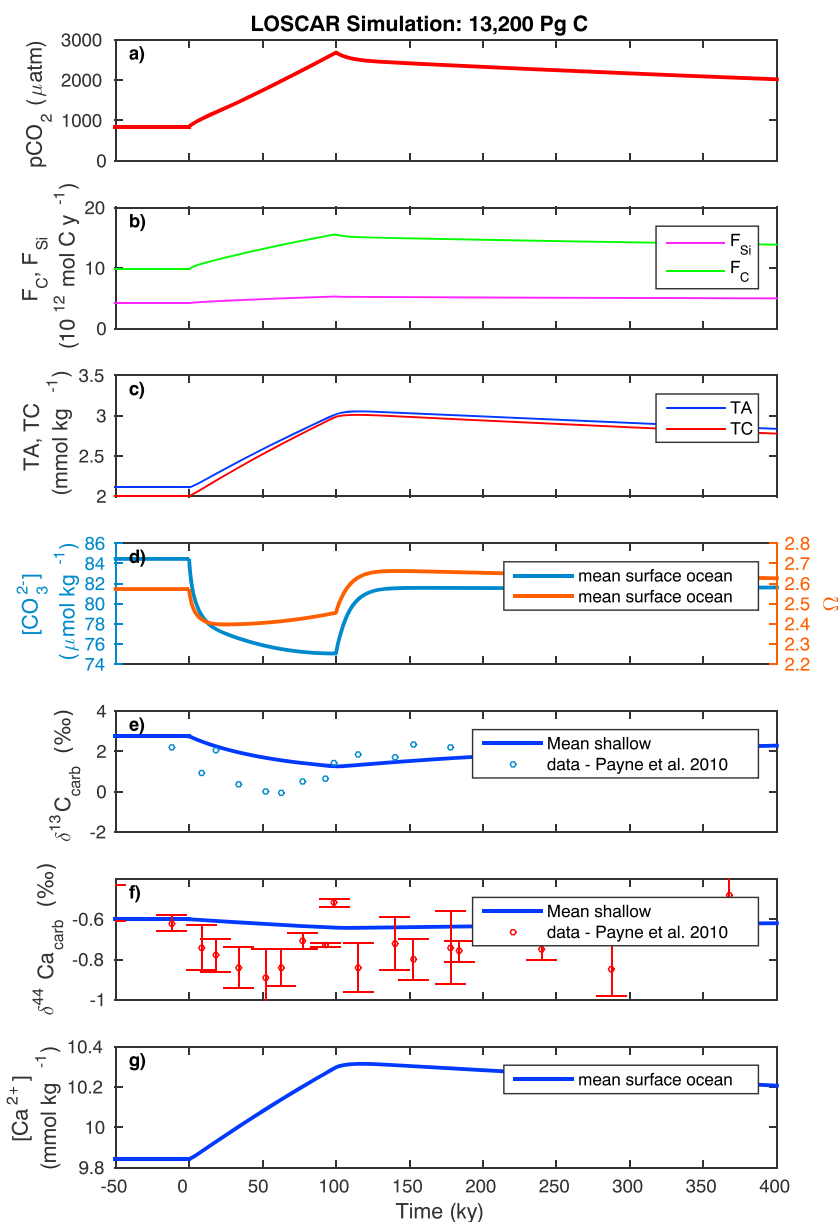


Figure 5. Forcing: 13,200 Pg C over 100 kyr (lower estimate proposed by Payne *et al.* [2010]). Weathering feedback parameters: $n_{CC} = 0.4$, $n_{Si} = 0.2$. (a) Predicted atmospheric CO_2 , (b) carbonate and silicate weathering fluxes (initial F_C and F_{Si} equal to 9.8 and $4.2 \times 10^{12} \text{ mol C yr}^{-1}$, respectively), (c) total alkalinity and total dissolved carbon, (d) mean surface ocean $[\text{CO}_3^{2-}]$ and calcite saturation, (e) mean $\delta^{13}\text{C}$ of shallow sediments, (f) mean $\delta^{44}\text{Ca}$ of shallow sediments, and (g) mean $[\text{Ca}^{2+}]$ of surface ocean.

where F_{Si} and F_C are silicate and carbonate weathering fluxes, respectively, and F_{Si}^0 and F_C^0 are the same fluxes at time $t = 0$. Similarly, $p\text{CO}_2^0$ is the initial ($t = 0$) atmospheric CO_2 concentration, and $p\text{CO}_2$ is the atmospheric partial pressure calculated in the model at time t . n_{Si} and n_{CC} are silicate and carbonate weathering $p\text{CO}_2$ feedback parameters, respectively, which determine the strength of the feedback. It follows that the carbon introduced into the system will eventually enhance the weathering rates, which is equivalent to increasing the riverine flux in the simple calcium model. Then, why do the two models produce significantly different responses?

In the simple model, the saturation state increases during the prescribed increase in weathering due to increased fluxes of Ca^{2+} and CO_3^{2-} ions, giving stronger saturation burial feedback (Figure 4). Therefore, any imbalance created by accelerated riverine input is quickly restored by enhanced burial resulting in a small

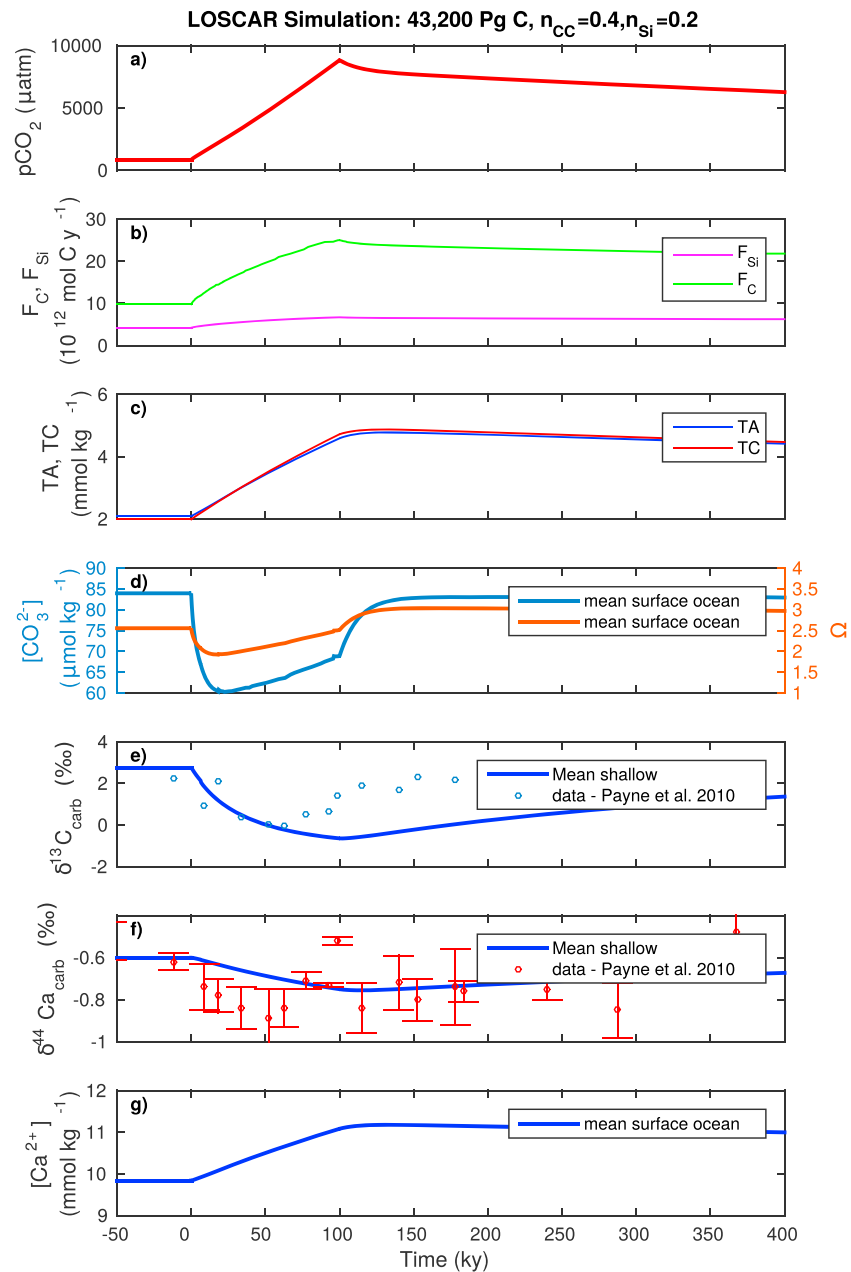


Figure 6. Forcing: 43,200 Pg C over 100 kyr (upper estimate proposed by Payne *et al.* [2010]). Weathering feedback parameters: $n_{CC}=0.4$, $n_{Si}=0.2$. (a) Predicted atmospheric CO_2 , (b) carbonate and silicate weathering fluxes (initial F_C and F_{Si} equal to 9.8 and $4.2 \times 10^{12} \text{ mol C yr}^{-1}$, respectively), (c) total alkalinity and total dissolved carbon, (d) mean surface ocean $[\text{CO}_3^{2-}]$ and calcite saturation, (e) mean $\delta^{13}\text{C}$ of shallow sediments, (f) mean $\delta^{44}\text{Ca}$ of shallow sediments, and (g) mean $[\text{Ca}^{2+}]$ of surface ocean.

change in $[\text{Ca}^{2+}]$ and $\delta^{44}\text{Ca}$. On the contrary, in LOSCAR, even though there is also an increase in weathering, the calcite saturation response is in the opposite direction (Figure 5d) when compared to the simple calcium model. Because LOSCAR includes complete ocean carbonate chemistry, the calcite saturation drops when a large input of carbon is introduced rapidly to the ocean-atmosphere system. As a result of a lower calcite saturation state, the dissolution rate of calcite increases dramatically, so there is essentially no burial. This state of accelerated weathering combined with practically no calcite burial augments the change in $[\text{Ca}^{2+}]$ and $\delta^{44}\text{Ca}_{\text{carb}}$ (Figures 5 to 7) when compared with the simple calcium model. The augmented change in $[\text{Ca}^{2+}]$ and $\delta^{44}\text{Ca}_{\text{carb}}$ predicted by LOSCAR is a more realistic response of the system. Nevertheless, even when an unrealistic mass of 43,200 Pg C is added to the ocean-atmosphere system over 100 kyr (the most extreme

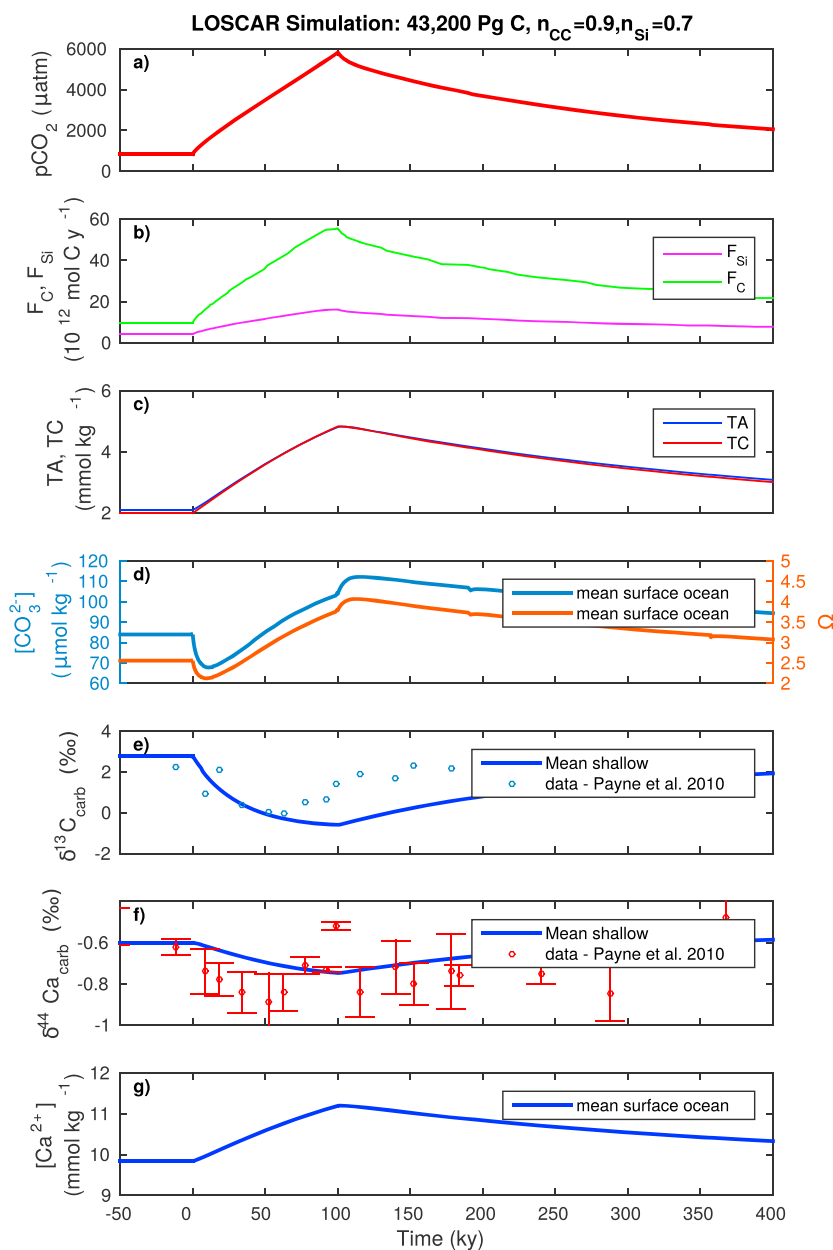


Figure 7. Forcing: 43,200 Pg C over 100 kyr (upper estimate proposed by Payne *et al.* [2010]). Weathering feedback parameters: $n_{CC}=0.9$, $n_{Si}=0.7$ (stronger feedback in order to get the same absolute increase in riverine fluxes as in Payne *et al.* [2010]). (a) Predicted atmospheric CO_2 , (b) carbonate and silicate weathering fluxes (initial F_C and F_{Si} equal to 9.8 and $4.2 \times 10^{12} \text{ mol C yr}^{-1}$, respectively), (c) total alkalinity and total dissolved carbon, (d) mean surface ocean $[\text{CO}_3^{2-}]$ and calcite saturation, (e) mean $\delta^{13}\text{C}$ of shallow sediments, (f) mean $\delta^{44}\text{Ca}$ of shallow sediments, and (g) Mean $[\text{Ca}^{2+}]$ of surface ocean.

scenario, Figure 7), the change in $\delta^{44}\text{Ca}_{\text{carb}}$ ($\Delta\delta^{44}\text{Ca} \sim 0.15\text{‰}$) is still not large enough to explain the observations (change of about 0.2‰ across the extinction horizon [Payne *et al.*, 2010]).

6. Alternative Hypothesis

The end-Permian extinction event is often associated with the formation of a large igneous province, namely, the Siberian Traps [e.g., Bowring *et al.*, 1998; Wignall, 2001; Kamo *et al.*, 2006]. The estimates of volume of basalt that was originally present in the Siberian Traps range from 2 to $4 \times 10^6 \text{ km}^3$ [Wignall, 2001; Lightfoot and Keays, 2005; Ivanov *et al.*, 2013]. According to McCartney *et al.* [1990], 1 km^3 of basalt emits $5 \times 10^{12} \text{ g}$ of C.

This translates to 10,000 to 20,000 Pg C that could have been released during the eruption of the Siberian Traps. As we show above, even as much as 40,000 Pg C would not have been enough to produce the desired change observed in $\delta^{44}\text{Ca}_{\text{carb}}$. Additional LOSCAR runs showed that around 70,000 Pg C of carbon would be necessary to achieve the desired drop of 0.2‰ in $\delta^{44}\text{Ca}_{\text{carb}}$ across the extinction horizon [Payne *et al.*, 2010]. Also, assuming that the age model used in Payne *et al.* [2010] is correct, then the carbon in the above LOSCAR simulations would have to be released at a much higher rate (≤ 50 kyr) in order to better match the observations. In turn, this would raise another issue; such a massive input of carbon would produce large and unrealistic atmospheric CO_2 concentration (10,000–20,000 ppm) [Cui and Kump, 2015]. It would also require a very high rate of carbon input, comparable to present-day anthropogenic emissions [Clarkson *et al.*, 2015], which appears difficult to imagine. According to our model, these problems indicate that the eruption of the Siberian Traps cannot alone reconcile all of the trends observed during end-Permian without consideration of additional feedbacks.

Rampino and Caldeira [2005] proposed an alternative mechanism which successfully reproduces the $\delta^{13}\text{C}$ and warming trends observed across the end-Permian without volcanic carbon input. They suggest that a drastic decrease in ocean primary productivity (“Strangelove Ocean”) was responsible for the observed negative excursion of $\sim 3\text{‰}$ (3.6‰ according to Payne *et al.* [2010]), and a consequent rise in $p\text{CO}_2$ was large enough to account for the observed warming of at least 6°C [Magaritz and Holser, 1991; Sun *et al.*, 2012]. The main assumption of Rampino and Caldeira [2005] was that the pre end-Permian $\delta^{13}\text{C}$ surface to deep gradient in the ocean was considerably greater than today, implying a significantly stronger biological carbon export during that time period when compared with the modern day ocean. Thus, shutting down the pre end-Permian biological pump (which was active prior to the extinction horizon) results in much greater rise in atmospheric $p\text{CO}_2$, when compared to similar model experiments for the modern ocean, in which $p\text{CO}_2$ increases from 280 μatm to around 500 μatm after turning off biological carbon export.

Here we perform an experiment in which initial export productivity in LOSCAR was set to approximately twice the modern value, similar to that of Rampino and Caldeira [2005], except that in our simulation marine biological export was linearly decreased to zero over the first 50 kyr, whereas Rampino and Caldeira [2005] turn off the biological pump instantaneously. The initial strength of biological carbon export is necessary in order to produce the observed Ca excursion and warming. The linear approach was chosen in order to obtain a better temporal match with the data (assuming that the age model used in Payne *et al.* [2010] is correct). The biological pump was then slowly and linearly returned to pre-perturbation level over the remainder of the simulation (~ 350 kyr). Additionally, Lemarchand *et al.* [2004] showed that in a simple inorganic system, the Ca isotope fractionation between calcite crystals and the mother solution directly depends on $[\text{CO}_3^{2-}]$ at which the crystals were precipitated. The regression line showing this dependence was calculated by Gussone *et al.* [2005] and was incorporated into LOSCAR:

$$1000 \cdot \ln(\alpha_{\text{cc}}) = -(1.31 \pm 0.12) + (3.69 \pm 0.59) \cdot [\text{CO}_3^{2-}] \text{ (mmol/kg)} \quad (9)$$

where $1000 \cdot \ln(\alpha_{\text{cc}})$ is the calcium isotope fractionation between calcium in solution and calcite in per mil. Therefore, fractionation between calcium in seawater and calcium carbonates becomes a function of $[\text{CO}_3^{2-}]$ during inorganic precipitation. In other words, the calcium isotope fractionation becomes larger as $[\text{CO}_3^{2-}]$ decreases and vice versa. The valid range of $[\text{CO}_3^{2-}]$ is 0 to 350 $\mu\text{mol kg}^{-1}$; hence, the range of $1000 \cdot \ln(\alpha_{\text{cc}})$ is -1.31 to 0‰ .

Slowing down and eventually turning off the biological carbon pump over 50 kyr elevates atmospheric $p\text{CO}_2$ via outgassing of CO_2 from the surface ocean (Figure 8a). Due to a sudden rise in $p\text{CO}_2$ (governed by equations (7) and (8)), silicate and carbonate weathering fluxes also increase (Figure 8b), which produces a small negative excursion in $\delta^{44}\text{Ca}$. The shutdown of the biological pump raises the amount of total dissolved carbon in the ocean at a faster rate than the rate of increase of total alkalinity (Figure 8c) causing the $[\text{CO}_3^{2-}]$ and calcite saturation to drop (Figure 8d). According to equation (9) this will result in a stronger calcium fractionation, which changes from the initial value of -0.92‰ to -1.09‰ (Figure 8f), affecting the $\delta^{44}\text{Ca}_{\text{carb}}$ and causing a larger negative excursion (faster input tempo (25 kyr as opposed to 50 kyr) of carbon produces only a slightly larger drop in $[\text{CO}_3^{2-}]$ and therefore does not affect the change in $\delta^{44}\text{Ca}$ significantly). Lower $[\text{CO}_3^{2-}]$ then leads to a reduction of shallow water carbonate deposition according to equation (6). Also, 12,000 Pg C with an isotopic composition of -5‰ was added to the ocean-atmosphere system over 50 kyr in order to

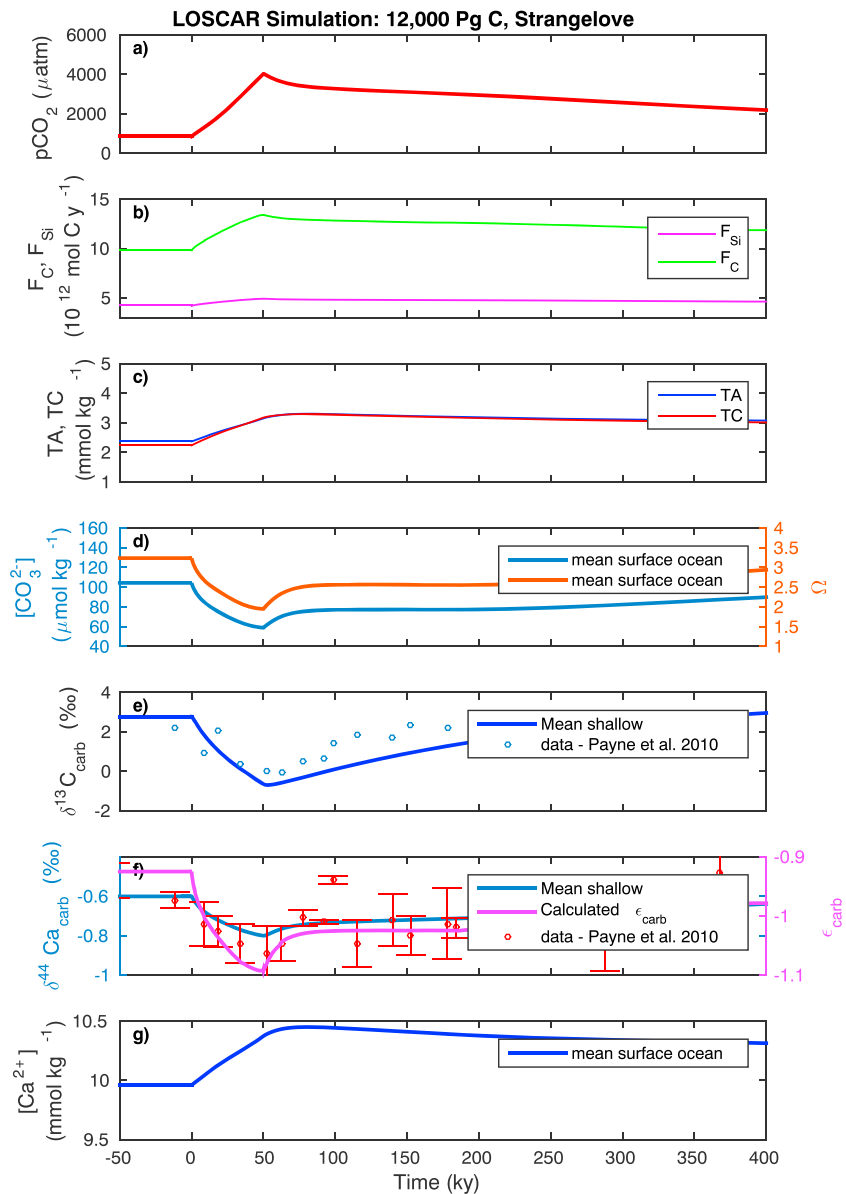


Figure 8. Simulation including Strangelove Ocean, C input (12,000 Pg), and variable calcium isotope fractionation (equation (9)). Weathering feedback parameters: $n_{CC}=0.2$, $n_{Si}=0.1$. (a) Predicted atmospheric CO_2 , (b) carbonate and silicate weathering fluxes (initial F_C and F_{Si} equal to 9.8 and $4.2 \times 10^{12} \text{ mol C yr}^{-1}$, respectively), (c) total alkalinity and total dissolved carbon, (d) mean surface ocean $[\text{CO}_3^{2-}]$ and calcite saturation, (e) mean $\delta^{13}\text{C}$ of shallow sediments, (f) Mean $\delta^{44}\text{Ca}$ of shallow sediments and calculated calcium isotope fractionation based on equation (9), and (g) mean $[\text{Ca}^{2+}]$ of surface ocean.

reproduce the full 0.2‰ change in $\delta^{44}\text{Ca}_{\text{carb}}$ (Figure 8f). The combination of the carbon input and the shut-down of the biological carbon pump leads to an increase of $p\text{CO}_2$ from the initial $850 \mu\text{atm}$ to $\sim 4000 \mu\text{atm}$, which translates into $>6^\circ\text{C}$ warming, assuming the canonical value of the fast-feedback sensitivity of 3°C [*IPCC*, 2007]. This temperature increase is consistent with temperature proxies for the end-Permian [*Magaritz and Holser*, 1991]. The amount of carbon introduced in this simulation (as calculated above) and its isotopic composition (-5‰) [*McLean*, 1986; *Kump and Arthur*, 1999] are also in line with the estimates associated with the Siberian Trap volcanism [*Wignall*, 2001; *Lightfoot and Keays*, 2005; *Ivanov et al.*, 2013]. Therefore, we propose the combined effect of the eruption of the Siberian Traps large igneous province, cessation of biological carbon export, and variable calcium isotope fractionation as a plausible mechanism responsible for the trends observed in $\delta^{13}\text{C}$, $\delta^{44}\text{Ca}$, and temperature across the end-Permian extinction event.

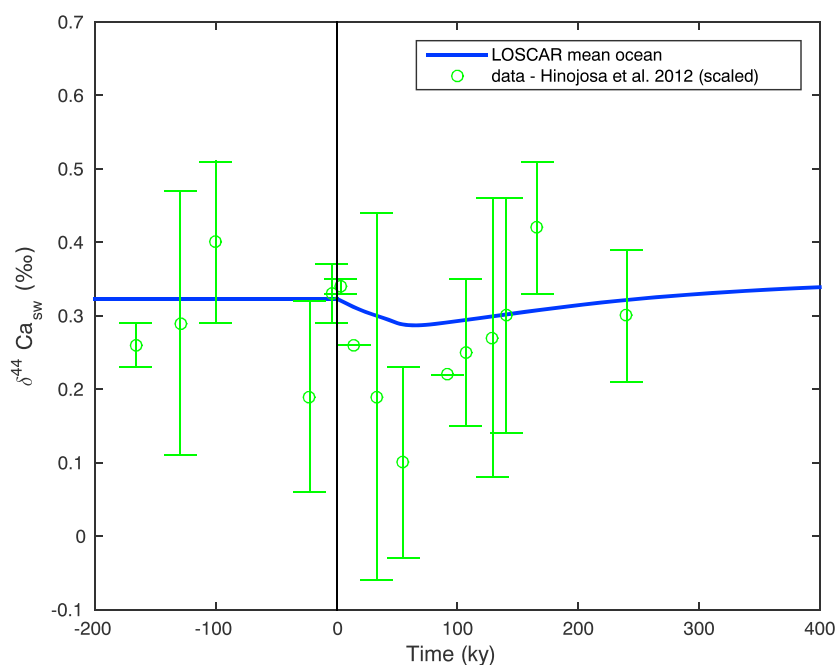


Figure 9. Evolution of $\delta^{44}\text{Ca}$ of seawater in LOSCAR for the simulation shown in Figure 8. Vertical black line marks the end-Permian extinction horizon. Open green circles are data from *Hinojosa et al.* [2012], shown in Figure 1, scaled to the model output by adding 1.05‰ to the measured values, so that the mean value of the preextinction data matches the preextinction value (0.32‰) of the model (see section 6.1). The conodont data are offset from seawater value and thus do not represent the absolute $\delta^{44}\text{Ca}_{\text{sw}}$ but rather the relative change.

6.1. Discussion

It is important to note that the $\delta^{44}\text{Ca}$ of seawater and $\delta^{44}\text{Ca}$ of carbonate rocks exhibit opposite trends (compared to one another) when the fluctuations are driven by changes in the fractionation factor (if the change in fractionation factor occurs over the time period that is shorter than the residence time of calcium). Therefore, during this transient period, the $\delta^{44}\text{Ca}_{\text{carb}}$ is not representative of the calcium isotopic composition of seawater (Figure S2) [Fantle, 2010; Fantle and Tipper, 2014]. This is different from the scenario in which fluctuations in $\delta^{44}\text{Ca}_{\text{sw}}$ are driven by changes in $\delta^{44}\text{Ca}$ of the weathering flux (or calcium imbalance between inputs and output fluxes) (Figure S3). Hence, in order to successfully reconstruct the $\delta^{44}\text{Ca}$ of the past and gain a better understanding of the calcium cycle, it would be necessary to have measurements of at least two distinct phases. One so called “passive” tracer that would reflect the changes in seawater $\delta^{44}\text{Ca}$ and the other that would constrain the $\delta^{44}\text{Ca}$ of buried carbonates [Fantle and Tipper, 2014]. *Hinojosa et al.* [2012] made such an attempt by measuring $\delta^{44}\text{Ca}$ of hydroxyapatite conodont microfossils ($\delta^{44}\text{Ca}_{\text{conodont}}$) across the end-Permian (passive tracer) complemented with $\delta^{44}\text{Ca}$ data of carbonate rock from the same time interval reported by *Payne et al.* [2010] (Figure 1). According to *Hinojosa et al.* [2012] the conodont calcium isotope data are representative of the seawater $\delta^{44}\text{Ca}$ variability across the end-Permian. The conodont data are offset from the seawater value and thus do not represent the absolute $\delta^{44}\text{Ca}_{\text{sw}}$ but rather the relative change. Because of rather large error bars, the data had to be statistically analyzed in order to make a meaningful comparison with the model results. A mean of $\delta^{44}\text{Ca}_{\text{conodont}}$ data along with the standard error of the mean before the extinction event was calculated ($-0.73 \pm 0.03\text{‰}$) and compared to the mean of the data ($-0.83 \pm 0.05\text{‰}$) that mark the isotope excursion (four data points right after the extinction horizon) (Figures 1 and S4). According to the statistical analysis, the change in $\delta^{44}\text{Ca}_{\text{conodont}}$ and therefore a change in $\delta^{44}\text{Ca}_{\text{sw}}$ could be anywhere between 0.02 and 0.18‰. This was then compared with the $\delta^{44}\text{Ca}_{\text{sw}}$ evolution predicted by the LOSCAR in our preferred scenario (Figures 8 and 9). The model calculated $\delta^{44}\text{Ca}_{\text{sw}}$ has the initial value of 0.32‰ which then exhibits a small negative excursion of about 0.04‰. The LOSCAR-predicted change in seawater isotopic composition presented here is therefore also consistent (within errors) with $\delta^{44}\text{Ca}_{\text{sw}}$ change predicted by the conodont microfossil data.

Additional model runs (Figure S5) were performed in order to test the model sensitivity to the following: (1) different residence times of calcium in the ocean as the residence time may have been different in the past

and (2) different $\delta^{44}\text{Ca}$ of the weathering flux as it might have also been different or it could change during the transient perturbation events by less than 0.3‰ [Fantle and Tipper, 2014]. The sensitivity runs indicate that neither different residence times of calcium nor a variable $\delta^{44}\text{Ca}$ of the weathering flux can significantly impact the model results on time scales of the end-Permian perturbation (see supporting information).

7. Conclusions

Several previous studies have employed a simple calcium-only model (following Payne *et al.* [2010]) with the attempt to resolve the dynamics and links between carbon and calcium cycles as well as the cause of the mass extinction during the end-Permian [Payne *et al.*, 2010; Hinojosa *et al.*, 2012] and more recently during the Toarcian oceanic anoxic event (Early Jurassic) [Brazier *et al.*, 2015]. Here we have identified the deficiencies in such a simplified approach and showed the importance of a fully coupled calcium-carbon cycle model.

The modeling framework presented here successfully reconciles the end-Permian trends in $\delta^{13}\text{C}$ and $\delta^{44}\text{Ca}$ recorded in carbonate sediments. The model also predicts a 50 kyr rise in atmospheric CO_2 causing a global temperature increase of more than 6°C. Our model results suggest that the end-Permian mass extinction and the perturbation in carbon-calcium cycling was due to a combination of several factors, including introduction of about 12,000 Pg of carbon through Siberian Trap volcanism, the collapse of ocean primary productivity, and a variable calcium isotope fractionation between seawater and buried carbonates during inorganic precipitation due to changing $[\text{CO}_3^{2-}]$. Most importantly, accelerated weathering rates alone that arise due to the perturbation in the carbon cycle are most likely insufficient to directly produce a significant impact on the calcium cycle, contrary to the claims of previous studies.

Acknowledgments

We would like to thank the two anonymous reviewers and Philip von Strandmann for their constructive criticism and valuable comments, which improved the manuscript. The $\delta^{13}\text{C}$ and $\delta^{44}\text{Ca}$ data used in this study are properly cited and referred to in the reference list. Any additional data produced by the model may be obtained from the corresponding author upon request (e-mail: komar@hawaii.edu).

References

- Amini, M., *et al.* (2008), Calcium isotope ($\delta^{44}/^{40}\text{Ca}$) fractionation along hydrothermal pathways, Logatchev field (mid-Atlantic Ridge, 14°45'N), *Geochim. Cosmochim. Acta*, 72(16), 4107–4122.
- Berner, R. A. (1994), GEOCARB II: A revised model of atmospheric CO_2 over Phanerozoic time, *Am. J. Sci.*, 294, 56–91.
- Berner, R. A. (1999), A new look at the long-term carbon cycle, *Geophys. Soc. Am. Today*, 9, 1–6.
- Bowring, S. A., D. Erwin, Y. Jin, M. Martin, K. Davidek, and W. Wang (1998), U/Pb zircon geochronology and tempo of the end-Permian mass extinction, *Science*, 280(5366), 1039–1045.
- Brazier, J.-M., G. Suan, T. Tacaill, L. Simon, J. E. Martin, E. Mattioli, and V. Balter (2015), Calcium isotope evidence for dramatic increase of continental weathering during the Toarcian oceanic anoxic event (Early Jurassic), *Earth Planet. Sci. Lett.*, 411, 164–176.
- Caldeira, K., and M. R. Rampino (1993), Aftermath of the end-Cretaceous mass extinction: Possible biogeochemical stabilization of the carbon cycle and climate, *Paleoceanography*, 8, 515–525.
- Clarkson, M., S. A. Kasemann, R. A. Wood, T. M. Lenton, S. J. Daines, S. Richoz, F. Ohnemüller, A. Meixner, S. W. Poulton, and E. T. Tipper (2015), Ocean acidification and the permo-Triassic mass extinction, *Science*, 348(6231), 229–232.
- Corsetti, F. A., A. Baud, P. J. Marengo, and S. Richoz (2005), Summary of Early Triassic carbon isotope records, *C. R. Palevol*, 4(6), 473–486.
- Cui, Y., and L. R. Kump (2015), Global warming and the end-Permian extinction event: Proxy and modeling perspectives, *Earth Sci. Rev.*, 149, 5–22.
- Elderfield, H., and A. Schultz (1996), Mid-ocean ridge hydrothermal fluxes and the chemical composition of the ocean, *Annu. Rev. Earth Planet. Sci.*, 24, 191–224.
- Erba, E. (2006), The first 150 million years history of calcareous nannoplankton: Biosphere–geosphere interactions, *Palaeogeogr. Palaeoclimatol. Palaeoecol.*, 232(2), 237–250.
- Erwin, D. H. (1993), *The Great Paleozoic Crisis: Life and Death in the Permian*, Columbia Univ. Press, New York.
- Fantle, M. S. (2010), Evaluating the Ca isotope proxy, *Am. J. Sci.*, 310, 194–230.
- Fantle, M. S., and D. J. DePaolo (2007), Ca isotopes in carbonate sediment and pore fluid from ODP Site 807A: The $\text{Ca}^{2+}(\text{aq})$ –calcite equilibrium fractionation factor and calcite recrystallization rates in Pleistocene sediments, *Geochim. Cosmochim. Acta*, 71(10), 2524–2546.
- Fantle, M. S., and E. T. Tipper (2014), Calcium isotopes in the global biogeochemical Ca cycle: Implications for development of a Ca isotope proxy, *Earth Sci. Rev.*, 129, 148–177.
- Grotzinger, J. P., and A. H. Knoll (1995), Anomalous carbonate precipitates: Is the Precambrian the key to the Permian?, *Palaios*, 10, 578–596.
- Gussone, N., F. Böhm, A. Eisenhauer, M. Dietzel, A. Heuser, B. M. Teichert, J. Reitner, G. Wörheide, and W.-C. Dullo (2005), Calcium isotope fractionation in calcite and aragonite, *Geochim. Cosmochim. Acta*, 69(18), 4485–4494.
- Hinojosa, J. L., S. T. Brown, J. Chen, D. J. DePaolo, A. Paytan, S.-z. Shen, and J. L. Payne (2012), Evidence for end-Permian ocean acidification from calcium isotopes in biogenic apatite, *Geology*, 40(8), 743–746.
- Holser, W. T., *et al.* (1989), A unique geochemical record at the Permian/Triassic boundary, *Nature*, 337(6202), 39–44.
- Horita, J., H. Zimmermann, and H. D. Holland (2002), Chemical evolution of seawater during the Phanerozoic: Implications from the record of marine evaporites, *Geochim. Cosmochim. Acta*, 66(1), 3733–3756.
- IPCC, I. P. o. C. C. (2007), *Climate Change 2007: The Physical Science Basis*, 996 pp., Cambridge Univ. Press, Cambridge, U. K.
- Ivanov, A. V., H. He, L. Yan, V. V. Ryabov, A. Y. Shevko, S. V. Paleskii, and I. V. Nikolaeva (2013), Siberian traps large igneous province: Evidence for two flood basalt pulses around the Permo-Triassic boundary and in the Middle Triassic, and contemporaneous granitic magmatism, *Earth Sci. Rev.*, 122, 58–76.
- Kamo, S., J. Crowley, and S. Bowring (2006), The Permian-Triassic boundary event and eruption of the Siberian flood basalts: An inter-laboratory U–Pb dating study, *Geochim. Cosmochim. Acta*, 70(18), A303.
- Knoll, A. H., R. Bambach, D. Canfield, and J. Grotzinger (1996), Comparative earth history and Late Permian mass extinction, *Science*, 273, 452–457.

- Knoll, A. H., R. K. Bambach, J. L. Payne, S. Pruss, and W. W. Fischer (2007), Paleophysiology and end-Permian mass extinction, *Earth Planet. Sci. Lett.*, *256*(3), 295–313.
- Komar, N., and R. E. Zeebe (2011), Changes in oceanic calcium from enhanced weathering did not affect calcium-based proxies during the Paleocene-Eocene Thermal Maximum, *Paleoceanography*, *26*, PA3211, doi:10.1029/2010PA001979.
- Kump, L. R., and M. A. Arthur (1999), Interpreting carbon-isotope excursions: Carbonates and organic matter, *Chem. Geol.*, *161*, 181–198.
- Lemarchand, D., G. J. Wasserburg, and D. A. Papanastassiou (2004), Rate-controlled calcium isotope fractionation in synthetic calcite, *Geochim. Cosmochim. Acta*, *68*(22), 4665–4678.
- Lightfoot, P. C., and R. R. Keays (2005), Siderophile and chalcophile metal variations in flood basalts from the Siberian Trap, Norilsk Region: Implications for the origin of the Ni-Cu-PGE sulfide ores, *Econ. Geol.*, *100*(3), 439–462.
- MacLeod, K. G., R. M. Smith, P. L. Koch, and P. D. Ward (2000), Timing of mammal-like reptile extinctions across the Permian-Triassic boundary in South Africa, *Geology*, *28*(3), 227–230.
- Magaritz, M., and W. T. Holser (1991), The Permian-Triassic of the Gartnerkofel-1 Core (Carnic Alps, Austria): Carbon and oxygen isotope variation, *Abh. Geol. Bundesanstalt*, *45*, 149–163.
- Magaritz, M., R. Krishnamurthy, and W. T. Holser (1992), Parallel trends in organic and inorganic carbon isotopes across the Permian/Triassic boundary, *Am. J. Sci.*, *292*(10), 727–739.
- McCarty, K., A. R. Huffman, and M. Tredoux (1990), A paradigm for endogenous causation of mass extinctions, *Geol. Soc. Am. Spec. Pap.*, *247*, 125–138.
- McLean, D. M. (1986), Mantle degassing unification of the Trans-K–T geobiological record, in *Evolutionary Biology*, edited by M. K. Hecht, B. Wallace, and G. T. Prance, pp. 287–313, Springer, New York.
- Opdyke, B. N., and B. H. Wilkinson (1993), Carbonate mineral saturation state and cratonic limestone accumulation, *Am. J. Sci.*, *293*, 217–234.
- Osen, A. K., A. M. Winguth, C. Winguth, and C. R. Scotese (2013), Sensitivity of Late Permian climate to bathymetric features and implications for the mass extinction, *Global Planet. Change*, *105*, 171–179.
- Payne, J. L., A. V. Turchyn, A. Paytan, D. J. DePaolo, D. J. Lehrmann, M. Yu, and J. Wei (2010), Calcium isotope constraints on the end-Permian mass extinction, *Proc. Natl. Acad. Sci. U.S.A.*, *107*(19), 8543–8548.
- Pilson, M. E. (2012), *An Introduction to the Chemistry of the Sea*, Cambridge Univ. Press, Cambridge, U. K.
- Rampino, M. R., and K. Caldeira (2005), Major perturbation of ocean chemistry and a “Strangelove Ocean” after the end-Permian mass extinction, *Terra Nova*, *17*(6), 554–559.
- Retallack, G. J. (1999), Postapocalyptic greenhouse paleoclimate revealed by earliest Triassic paleosols in the Sydney Basin, Australia, *Geol. Soc. Am. Bull.*, *111*(1), 52–70.
- Ridgwell, A. (2005), A mid Mesozoic revolution in the regulation of ocean chemistry, *Mar. Geol.*, *217*, 339–357.
- Ridgwell, A., and R. E. Zeebe (2005), The role of the global carbonate cycle in the regulation and evolution of the Earth system, *Earth Planet. Sci. Lett.*, *234*, 299–315.
- Ridgwell, A. J., M. J. Kennedy, and K. Caldeira (2003), Carbonate deposition, climate stability, and Neoproterozoic ice ages, *Science*, *302*(5646), 859–862.
- Royer, D. L., R. A. Berner, I. P. Montanez, N. J. Tabor, and D. J. Beerling (2004), CO₂ as a primary driver of Phanerozoic climate change, *Geophys. Soc. Am. Today*, *14*(3), 4–10.
- Skulan, J., D. J. DePaolo, and T. L. Owens (1997), Biological control of calcium isotopic abundances in the global calcium cycle, *Geochim. Cosmochim. Acta*, *61*(12), 2505–2510.
- Sun, Y., M. M. Joachimski, P. B. Wignall, C. Yan, Y. Chen, H. Jiang, L. Wang, and X. Lai (2012), Lethally hot temperatures during the Early Triassic greenhouse, *Science*, *338*(6105), 366–370.
- Urey, H. C. (1952), *The Planets: Their Origin and Development*, p. 245, Yale Univ. Press, New Haven, Connecticut.
- Walker, L. J., B. H. Wilkinson, and L. C. Ivany (2002), Continental drift and phanerozoic carbonate accumulation in shallow-shelf and deep-marine settings, *J. Geol.*, *110*(1), 75–87.
- Wignall, P. (2001), Large igneous provinces and mass extinctions, *Earth Sci. Rev.*, *53*(1), 1–33.
- Wignall, P. B., and R. Newton (2003), Contrasting deep-water records from the upper Permian and lower Triassic of South Tibet and British Columbia: Evidence for a diachronous mass extinction, *Palaio*, *18*(2), 153–167.
- Woods, A. D., D. J. Bottjer, M. Mutti, and J. Morrison (1999), Lower Triassic large sea-floor carbonate cements: Their origin and a mechanism for the prolonged biotic recovery from the end-Permian mass extinction, *Geology*, *27*(7), 645–648.
- Zeebe, R. E. (2012), LOSCAR: Long-term ocean-atmosphere-sediment carbon cycle reservoir model v2.0.4, *Geosci. Model Dev.*, *1*, 149–166.
- Zeebe, R. E., and P. Westbroek (2003), A simple model for the CaCO₃ saturation state of the ocean: The “Strangelove”, the “Neritan”, and the “Cretan” Ocean, *Geochem. Geophys. Geosyst.*, *4*(12), 1104, doi:10.1029/2003GC000538.
- Zeebe, R. E., and D. A. Wolf-Gladrow (2001), CO₂ in Seawater: Equilibrium, Kinetics, Isotopes, p. 346, Elsevier Oceanogr. Ser., Elsevier, Amsterdam.
- Zhu, P., and J. D. Macdougall (1998), Calcium isotopes in the marine environment and the oceanic calcium cycle, *Geochim. Cosmochim. Acta*, *62*(10), 1691–1698.